Can a Hencky-Type Model Predict the Mechanical Behaviour of Pantographic Lattices?

Emilio Turco, Maciej Golaszewski, Ivan Giorgio and Luca Placidi

Abstract Current research in metamaterials design is pushing to fill the gap between mathematical modeling and technological applications. To meet these requirements, predictive and computationally effective numerical tools need to be conceived and applied. In this paper we compare the performances of a discrete model already presented in [1], strongly influenced by Hencky approach [2], versus some interesting experiments on pantographic structures built using the 3D printing technology. The interest in these structures resides in the exotic behavior that they have already shown, see [3, 4], and their study seems promising. In this work, after a brief presentation of the discrete model, we discuss the results of three experiments and compare them with the corresponding predictions obtained by the numerical simulations. An in-depth discussion of the numerical results reveals the robustness of the numerical model but also clearly indicates which are the focal points that strongly influence the accuracy of the numerical simulation.

E. Turco
Department of Architecture, Design and Urban Planning,
via Garibaldi 35, Alghero, Italy
e-mail: emilio.turco@uniss.it

M. Golaszewski
DCEBM, Warsaw University of Technology, Warsaw, Poland
e-mail: golaszewski.maciej07@gmail.com

I. Giorgio
MeMoCS, International Research Center for the Mathematics and
Mechanics of Complex Systems, Università dell'Aquila, L'Aquila, Italy
e-mail: ivan.giorgio@uniroma1.it

L. Placidi (✉)
Faculty of Engineering, International Telematic University Uninettuno,
Rome, Italy
e-mail: luca.placidi@uninettunouniversity.net

F. dell'Isola et al. (eds.), *Mathematical Modelling in Solid Mechanics*,
Advanced Structured Materials 69, DOI 10.1007/978-981-10-3764-1_18

1 Introduction

Current research in metamaterials design is pushing to fill the gap between mathematical modeling and technological applications. Although both evolutionary selection in living organism and the past engineering scientifically based research have already promoted the conception of *exotic* metamaterials (the bone tissue is one example while woven fabrics gives another one) it is only a recent issue the systematic research of tailored materials having fixed well-determined a priori uses and applications. To meet all the requirements imposed by determined and well-specified applications it is needed to establish a designing procedure which involve the important step concerning the development of some predictive and computationally effective numerical tools. These tools will be then used to verify experimental measurements output and subsequently to design specifically adapted materials.

In this paper we focus on a specific, but in our opinion relevant, task: to compare the performances of a discrete model for pantographic lattices, sometimes also called pantographic sheets, with some interesting experiments. The interest in these structures resides in the exotic behavior that they have shown [3, 4] and their study seems promising. In particular pantographic structures:

- are the actual realization of a (often disputed) continuum model: i.e. second gradient materials; indeed pantographic sheets are one of the first mechanical structures which have been proven, see [5], to need a second gradient models at a given macroscopic length-scale;
- have been proven to have very promising properties in wave propagation, representing an example of effective wave-guides, see [6];
- have shown promising toughness properties, which suggest that they could be fruitfully embedded in novel composite materials.

The comparison between an effective discrete model and some experiments shows, on one side, its robustness and, on the other side, the focus points which require strong attention when accurate results are desired.

In the following we briefly present the discrete model, Sect. 2, also mentioning the algorithm used to reconstruct the complete equilibrium path of the mechanical problem. Successively, in Sect. 3, we thoroughly discuss some experiments and the comparison with the corresponding numerical simulations. Finally, in Sect. 4, there are some concluding remarks and future perspectives.

2 Discrete Model for Pantographic Sheets

In this section we shortly describe the discrete Lagrangian model which we consider here to be possible model for planar pantographic structures. Their predictive performances will be analysed in the following Sect. 3. We limit ourselves to remark here that:

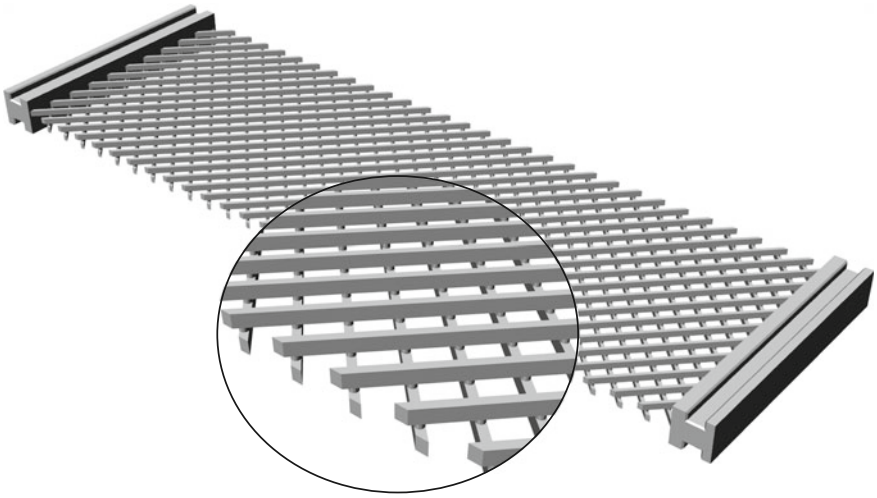

Fig. 1 Pantographic structure fabric built by using 3D printing technology

- pantographic structures can be nowadays simply built using 3D printing technologies (see, e.g., Fig. 1) based on the concept first proposed in [4] where elastic pivots were realized with small size elastic cylinders interconnecting the two arrays of beams;
- discrete models, see Fig. 2, are conceived by modelling interconnecting pivots as nodes linked each other by means of extensional (pairwise interaction, see Fig. 3a) and rotational springs, i.e. bending springs (triple interaction on a fiber, see Fig. 3b) and shear springs (triple interaction on a fiber of the same array and also on the nearest pivots on the other direction, see Fig. 3c).

The kinematical description of the pantographic lattice model involves a finite configuration space. To be precise, the discrete model involves the introduction of a set of Lagrangian parameters specifying the position of all the material particles modelling the pivots. They are initially located in the nodes of the reference configuration and then they displace in the actual configuration. If we limit ourself to consider planar motions, only a set of $2N$ coordinates is sufficient (if N is the number of considered nodes, the generic of which has referential position given by $P_{i,j}$, such a set of Lagrangian coordinates could be given by the corresponding actual position $p_{i,j}$).

The strain energies of the discrete model are the only kind of energy to be specified in hard devices deformations (in absence of relevant volume forces). The postulated expression for the Lagrangian discrete deformation energy W_{int} (in terms of the Lagrangian coordinates $p_{i,j}$) is completely defined specifying the contribution of each one kind of spring (see Figs. 2 and 3):

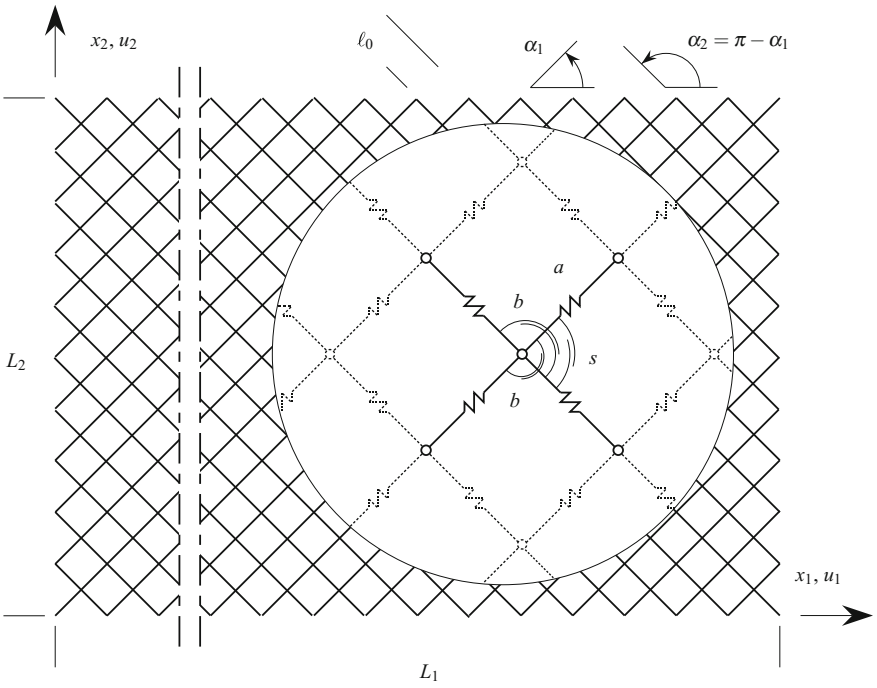

Fig. 2 Hencky-type mechanical model of a pantographic structure

$$w_a = \frac{1}{2}a(\ell - \ell_0)^2\,, \tag{1}$$

$$w_b = b(\cos\beta + 1)\,, \tag{2}$$

$$w_s = \frac{1}{2}s(\sigma - \sigma_0)^2\,, \tag{3}$$

where ℓ and ℓ_0 are the actual and the reference length, respectively, of pantographic bar (i.e. the distance between two consecutive pivots along fibers' direction), β is the angle between two consecutive pantographic bars (in the reference configuration this angle is π) and σ is the angle between two fibers starting from the same pivot (in the reference configuration this angle is related to α_1 or α_2 and σ_0). Furthermore, a, b and s are the axial, bending and shear stiffnesses of each one type of spring, respectively.

Some remarks:

i. The shear springs used for the discrete model, and depicted in Figs. 2 and 3, are actually four, having the same stiffness, for each node or pivot, one for each quadrant and having origin, in the reference configuration, at $P_{i,j}$.
ii. The bending deformation energy is expressed by means of the $\cos\beta$ instead of the corresponding angle β, these two possibilities are equivalent, at least in principle,

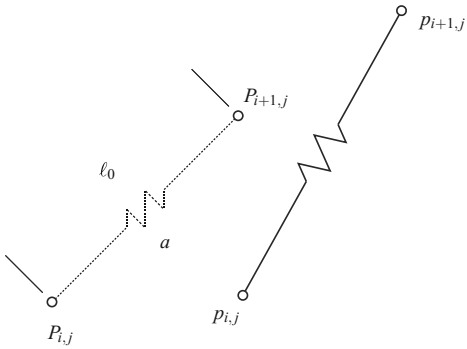

(a) axial spring

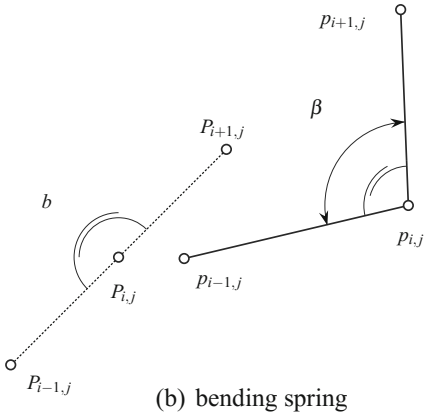

(b) bending spring

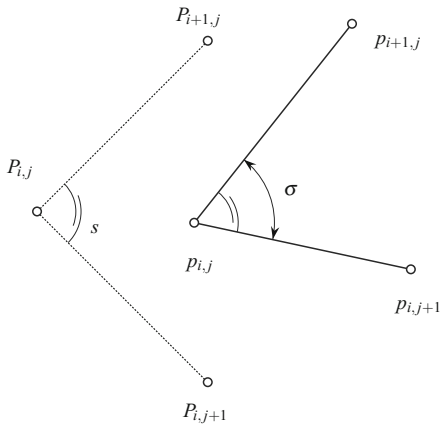

(c) shear spring

Fig. 3 Kinematics of axial (**a**), bending (**b**) and shear (**c**) springs: reference (*dashed line*) and actual (*continuous line*) configurations

but the first, avoiding the use of arccos(·) function, results more convenient from the computational point of view since it produces a more compact and effective code.

In order to have a complete solution of the considered equilibrium problem, i.e. the displacements (from which can be easily evaluated the structural reaction and the forces or couples exerted by each spring) a step-by-step procedure was implemented to reconstruct the complete equilibrium path of the pantographic sheet.

We briefly sketch here the basic ingredients of the procedure. The total energy of the pantographic structure can be computed in a straightforward manner simply adding the strain contribution of each spring. Formally we can write:

$$W(\mathbf{d}) = W_{\text{int}} - W_{\text{ext}} = \sum_{e} (w_a + w_b + w_s) - W_{\text{ext}} \,, \tag{4}$$

where e ranges on all the springs, extensional, bending and shear, and W_{ext} is the work of the external loads and all quantities on the *RHS* depend on the vector $\mathbf{d}$ which collects the nodal displacements of the pantographic lattice.

The equilibrium problem which we want to consider is a mixed one: we assume that the displacements of some particles are imposed and that some externally conservative forces are applied to the remaining particles. Let us therefore decompose $\mathbf{d}$ into the pair composed by two vectors: the assigned displacements $\mathbf{u}_a$ and the free displacements $\mathbf{u}$. For notational aims, we will reorder $\mathbf{d}$ to get the decomposition

$$\mathbf{d} = (\mathbf{u}, \mathbf{u}_a) \ .$$

Because of our assumption we have that W_{ext} depends only on $\mathbf{u}$.

The nonlinear system of equilibrium equations is obtained by imposing that the first variation of W vanish:

$$\mathbf{s}(\mathbf{u}) - \mathbf{p}(\mathbf{u}) = \mathbf{0} \,, \tag{5}$$

where $\mathbf{p}(\mathbf{u})$ is the vector which collects the Lagrangian components of external forces (which may be assumed to be dead loads, for instance, so that $\mathbf{p}$ becomes independent of $\mathbf{u}$) and $\mathbf{s}(\mathbf{u})$ is the vector of the internal forces (called also, in the context of structural mechanics, *structural reaction*), as defined by:

$$\mathbf{s}(\mathbf{u}) = \frac{\mathrm{d}W_{\text{int}}}{\mathrm{d}\mathbf{u}} \,, \qquad \mathbf{p}(\mathbf{u}) = \frac{\mathrm{d}W_{\text{ext}}}{\mathrm{d}\mathbf{u}} \,. \tag{6}$$

The tangent stiffness matrix is defined as the derivative of the structural reaction $\mathbf{s}(\mathbf{u})$ with respect to the displacement vector $\mathbf{u}$, in formulas:

$$\mathbf{K}_T(\mathbf{u}) = \frac{\mathrm{d}\mathbf{s}(\mathbf{u})}{\mathrm{d}\mathbf{u}} = \frac{\mathrm{d}^2 W_{\text{int}}}{\mathrm{d}\mathbf{u}^2} \,, \tag{7}$$

The solution of the nonlinear equilibrium system of Eq. (5) can be found by means of an incremental-iterative procedure based on the Newton–Raphson scheme.

Table 1 Scheme of a basic algorithm to compute a new point of the equilibrium path $(\lambda_{j+1}, \mathbf{u}_{j+1})$ given the previous $(\lambda_j, \mathbf{u}_j)$

set	
exit := false	
$\mathbf{K}_T := \mathbf{K}_T(\mathbf{u}_j)$	
$\Delta\mathbf{u} := \Delta\lambda\bar{\mathbf{u}}$	($\bar{u} = 0$ for free nodes and $\bar{u} = u_a$ for the assigned ones)
while (loop < maxloop) and (exit=false)	
$\mathbf{s} := \mathbf{s}(\mathbf{u}_j + \Delta\mathbf{u})$	
$\dot{\mathbf{u}} := \mathbf{K}_T^{-1}\mathbf{s}$	
if $\|\dot{\mathbf{u}}\| > \eta$	
$\Delta\mathbf{u} := \Delta\mathbf{u} - \dot{\mathbf{u}}$	
$\mathbf{K}_T := \mathbf{K}_T(\mathbf{u}_j + \Delta\mathbf{u})$	
else	
exit := true	
end	
save	
$\lambda_{j+1} := \lambda_j + \Delta\lambda$	
$\mathbf{u}_{j+1} := \mathbf{u}_j + \Delta\mathbf{u}$	

We will limit ourselves to the case of equilibrium paths depending only by the single parameter λ. Starting from an estimated point of the equilibrium path $(\lambda_j, \mathbf{u}_j)$ verifying that the residue $\mathbf{r}$ of Eq. (5) is

$$\left\|\mathbf{r}(\mathbf{u}_j, \lambda_j)\right\| \leq \eta\,, \tag{8}$$

i.e.with a pair being an η-approximate solution of the equilibrium condition (5), the iterative scheme, once the step $\Delta\lambda$ is fixed, is obtained by constructing the η-approximate solution $(\mathbf{u}_{j+1} =: \mathbf{u}_j + \Delta\mathbf{u}_j\,, \lambda_{j+1} := \lambda_j + \Delta\lambda)$ by using the iteration scheme reported in Table 1 to compute $\Delta\mathbf{u}_j$.

Further details on the Hencky-type model and on the strategy used to compute the complete equilibrium path are contained in [1], in addition [7–9] report a comparison of numerical simulations, also with second gradient numerical model, with experimental results in the case of fiber push-out and extensional and bending cases.

3 Comparison with Experiments

The reader will remark that very few parameters are postulated to characterize the discrete model. On the contrary a wealth of experimental data are nearly perfectly fitted using these few parameters. In [3] an identification of the parameters of the continuum model in terms of the discrete model was proposed, see [5, 10, 11].

Below we consider three experiments performed on specimen built by using 3D printing technologies. Each one test is characterized by a different orientation of the fibers. By referring to Fig. 2, the first one considers the case $\alpha_1 = \pi/4$, the second one $\alpha_1 = \pi/6$ and the last one $\alpha_1 = \pi/3$. We remark that in the first case the fibers are orthogonal, contrarily to the second and third case. Another remarkable difference regards the boundary conditions. More precisely, in the first test the same extensional displacements have been assigned only on two fibers of the small side (using a small bridge, see subsection 3.1) whereas in the other cases, see subsections 3.2 and 3.3, the displacements are assigned on all the fibers which intersect the small side.

3.1 Fiber Push-Out Test

On the basis of the technical drawing reported in Fig. 4, a specimen was built, by using the 3D printing technology, in polyamide (PA 2200) by a SLS Formiga P100. The Young's modulus for this material was estimated between 1.5 and 1.7 GPa following the rules of EN ISO 527 and EN ISO 178.

This specimen was tested by clamping the entire left side and assigning an increasing displacement u (parallel to the larger sides) to two fibers of the right side until

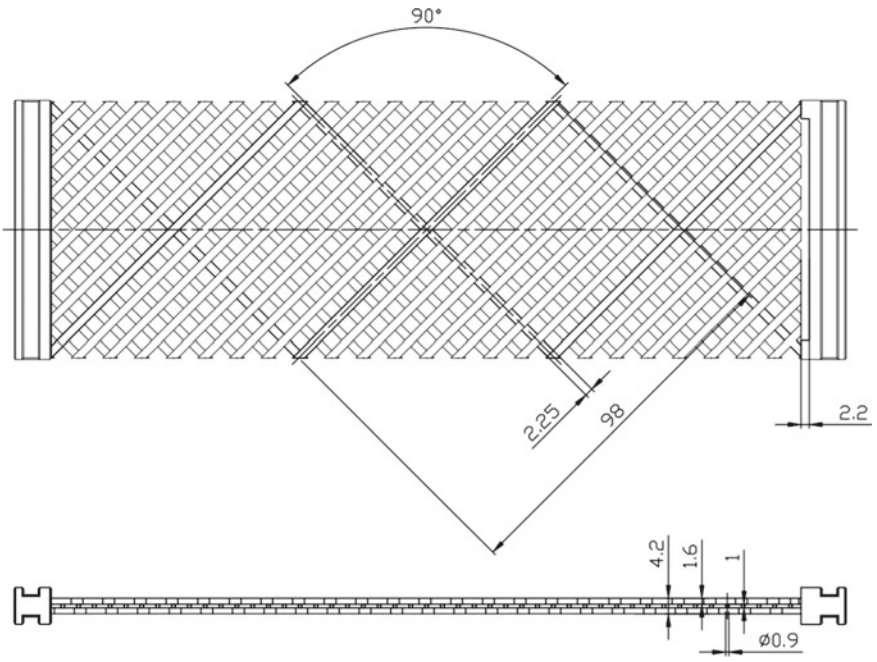

Fig. 4 Drawing of the specimen for the fiber push-out test

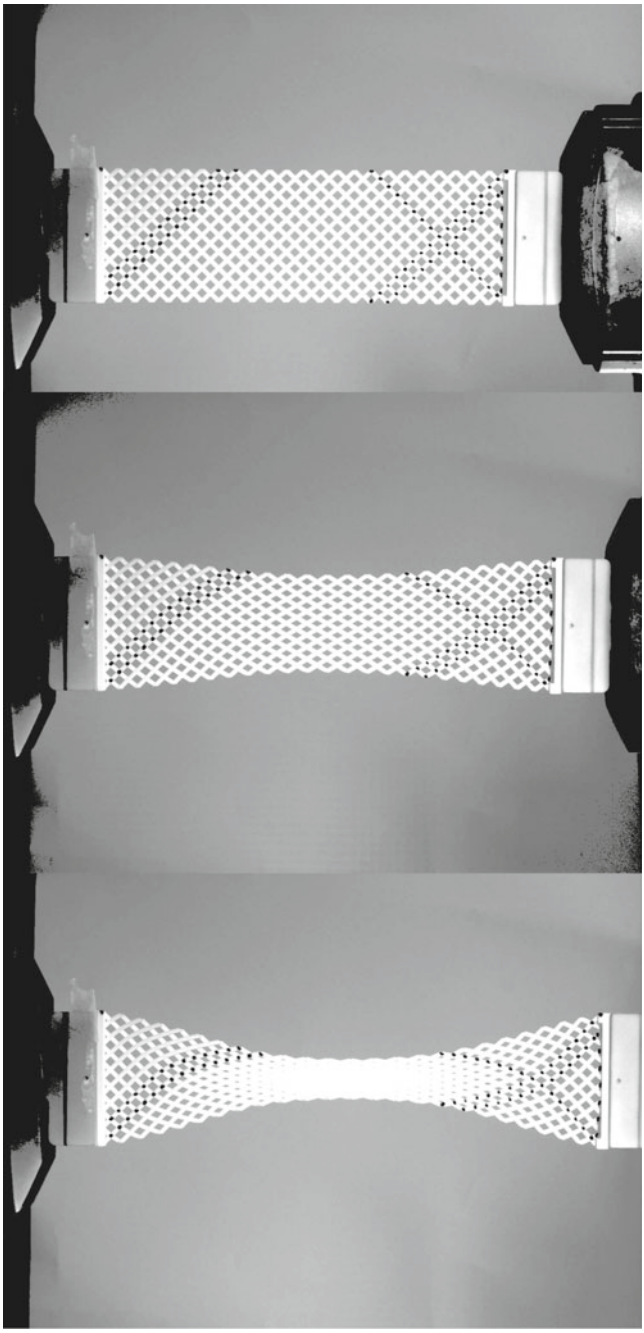

Fig. 5 Push-out test: sequence of deformations for $\lambda = 0, 0.5$ and 1

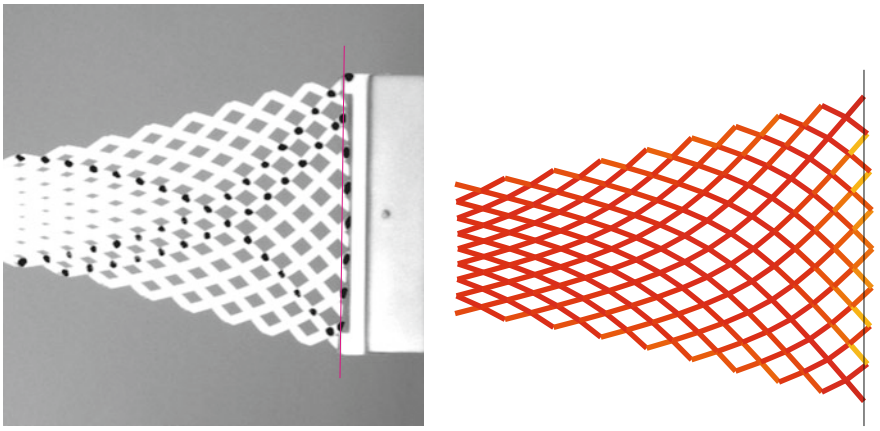

(a) experiments (b) numerical simulation

Fig. 6 Push-out test: particular of the deformation near the push-out fibers

Table 2 Spring stiffnesses consequent to different values of the Young's modulus

E (GPa)	a (N/mm)	b_1 (Nmm)	b_2 (Nmm)	s (Nmm)
1.6	265.0	238.2	238.2	0.9739
1.2	198.8	178.7	148.9	0.7304

its maximum $u_{\max}$ was reached by using the MTS Bionix system strength machine selecting a velocity of about 5 mm/min. From the drawing, it is clear that the assigned displacement engages only on two fibers thanks to the small bridge on the right side. We remark the there is a small gap, i.e. 2.2 mm, between the fibers and the small bridge on the right side. The reasons of this gap will be better clarified in the following.

Figure 5 reports three pictures taken during the test execution and distinct for the displacement parameter $\lambda = u/u_{\max}$. It has to be highlighted the particular effect reported in Fig. 6a which makes clear the necessity of the gap on the specimen.

Numerical simulation of this test was performed by assuming for the spring stiffnesses the same values already used in [7] for similar specimens. These values are reported in the first row of Table 2 and correspond to the value of the Young's modulus $E = 1.6$ GPa (an intermediate value of the declared range) estimated by using the suggestion reported in [12].

In Fig. 7a is reported the comparison between the structural reaction on the left side of the specimen both for the experiment, in black, and for the numerical simulation, in red. The uncertainties on E and the awareness that this parameter could hardly affects all the stiffness parameters, see e.g. [8, 9, 13] for some insights, suggested us for trying to improve the curve fitting simply modifying the Young's modulus, and consequently the stiffness parameters of the springs. A surely better fitting was

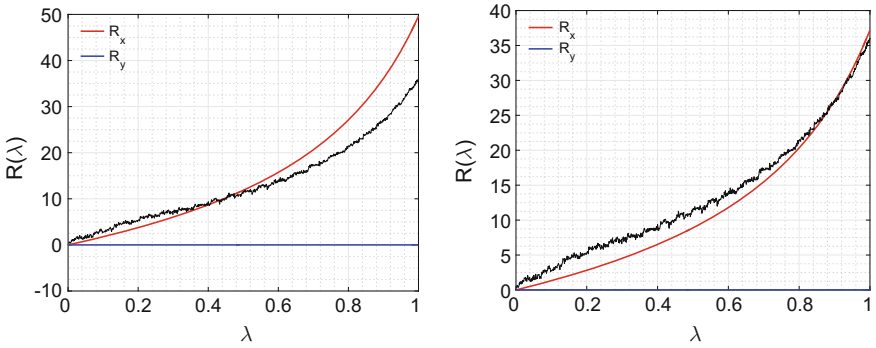

(a) $E = 1.6$ GPa (b) $E = 1.2$ GPa

Fig. 7 Push-out test: structural reaction for different values of the Young's modulus

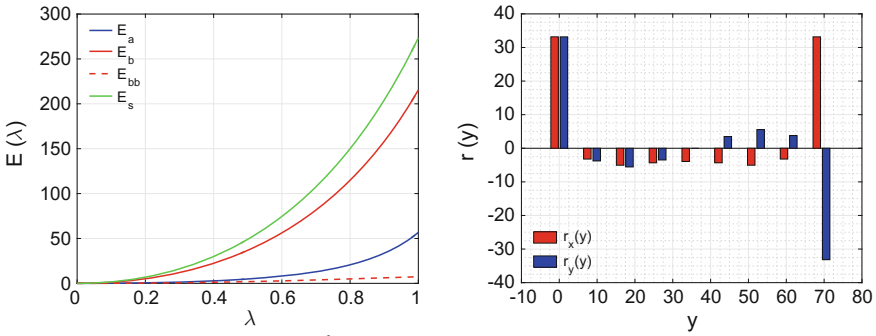

(a) Energy E *vs.* λ (b) Density of structural reaction r on the side $x_1 = 0$ for $\lambda = 1$

Fig. 8 Push-out test: energy, structural reaction and its density computed by using the Hencky-type numerical model

obtained using $E = 1.2$ GPa, see Fig. 7b, and the consequent stiffness parameters of the springs, see the second row of Table 2. For this value of E, and for the consequent springs stiffnesses, we also report in Fig. 8 both the strain energy, distinct for axial, bending and shear, as λ increases and the density of the structural reaction on the left side. Particularly remarkable is the presence of negative (red) values which indicate compressions on the most of the center of the side.

Figure 9 reports the deformations as λ increases, in particular for the cases $\lambda = 0.25, 0.5, 0.75$ and 1. In grey is reported the reference configuration whereas colors shows the density of the achieved energy level.

Finally, we observe that the numerical simulation reproduces, see Fig. 6b, the same remarkable effect reported in Fig. 6a.

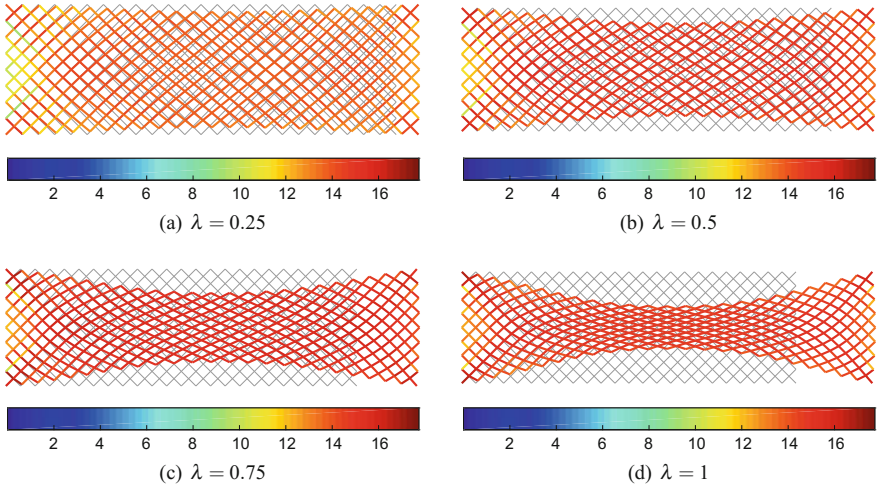

Fig. 9 Push-out test: deformations by using the Hencky-type numerical model

It has to be remarked that the used springs stiffnesses give quite satisfactory results for what concerns the structural reaction fitting. Conversely, looking at the contraction in the central part of the specimen, the numerical simulation appears more thick than that detected during in the experiment. The reason of this difference is probably due to a non precise choice of the constitutive parameters used in the numerical simulations.

3.2 Pantograph with Non-orthogonal Fibers: $\alpha_1 = \pi/6$

This test concerns the specimen depicted in Fig. 10. In this case the most remarkable thing is the lack of orthogonality between intersecting fibers.

Also in this case the specimen was built using the polyamide in the 3D printing process. In this case both the left and right side are clamped and an assigned displacement u, parallel to the larger side of the specimen, was imposed on the right side until the value $u_{\max} = 23.7$ mm. Using the same strength machine and the same assigned velocity (5 mm/min), the three pictures, distinct by the displacement parameter $\lambda = u/u_{\max}$, were taken, see Fig. 11.

The experience of the previous test suggested us to choose the springs stiffnesses using, as a fitting rule, the agreement between the deformations at the final stage both for the experiments and for the numerical simulations. This choice leads to the springs stiffnesses reported in Table 3.

Using these values for springs stiffnesses we obtained the results reported in Fig. 12 where we reported the energies and the structural reactions vs λ and the density of the structural reaction, for $\lambda = 1$, on the left side of the specimen. In

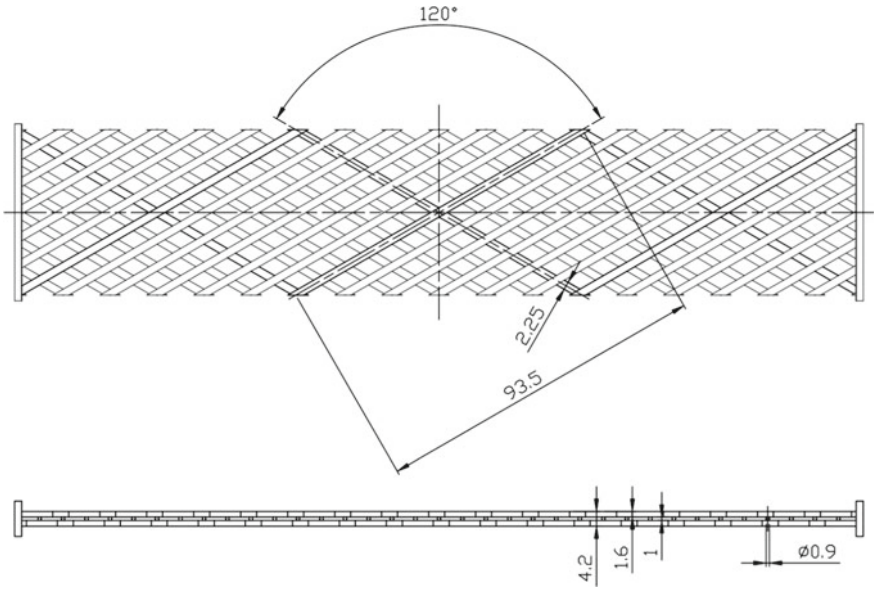

Fig. 10 Drawing of a pantographic structure with non-orthogonal fibers: $\alpha_1 = \pi/6$

Table 3 Stiffnesses of the springs

a (N/mm)	b_1 (Nmm)	b_2 (Nmm)	s (Nmm)
165.6	148.9	148.9	0.977

Fig. 12b there is the comparison between the structural reaction evaluated during the experiment, in black, and that computed by the numerical simulation, in red. The closeness of the two curves it is remarkable.

The deformation history computed by using the numerical model is reported in Fig. 13 for $\lambda = 0.25, 0.5, 0.75$ and 1.

Finally we reported in Fig. 14 an overlapping of the picture taken at the final deformation of the experiment and that computed numerically which clearly shows the quality of the numerical model when an accurate fitting of the spring stiffnesses is preventively performed.

3.3 Pantograph with Non-orthogonal Fibers: $\alpha_1 = \pi/3$

The last test concerns again a specimen made by the same polyamide of the previous tests and with non-orthogonal fibers but this time with a different orientation, see the drawing reported in Fig. 15.

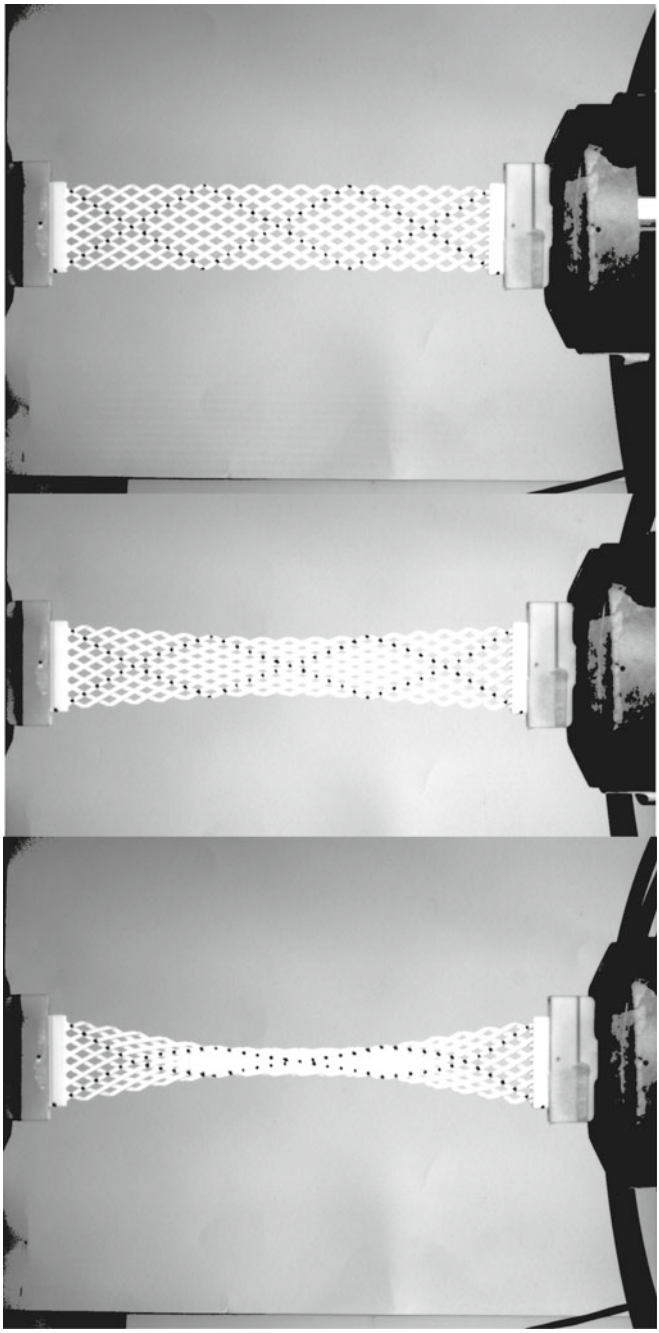

Fig. 11 Pantograph with non-orthogonal fibers ($\alpha_1 = \pi/6$): sequence of deformations for $\lambda = 0$, 0.5, 1

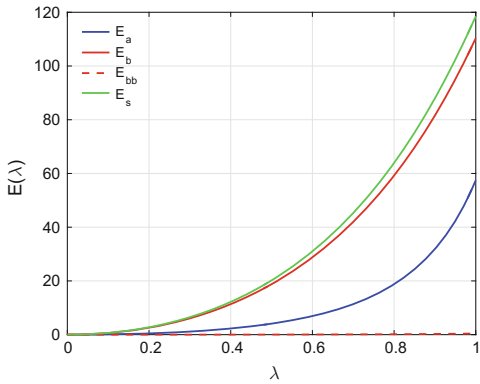

(a) Energy E *vs.* λ

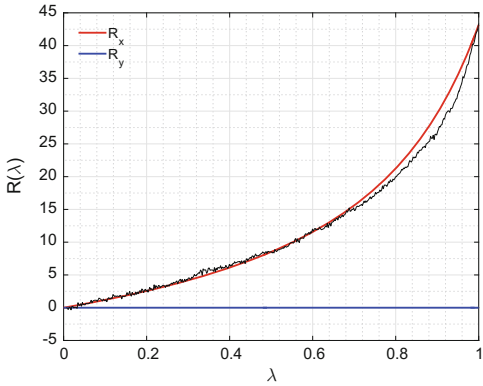

(b) Structural reaction R *vs.* λ
(in black is reported the experimental result)

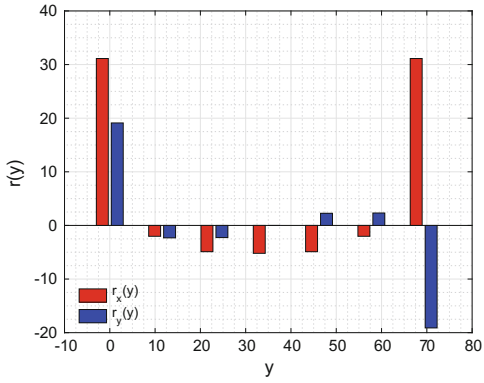

(c) Density of structural reaction r
on the side $x_1 = 0$ for $\lambda = 1$

Fig. 12 Pantograph with non-orthogonal fibers ($\alpha_1 = \pi/6$): energy, structural reaction and its density computed by using the Hencky-type numerical model

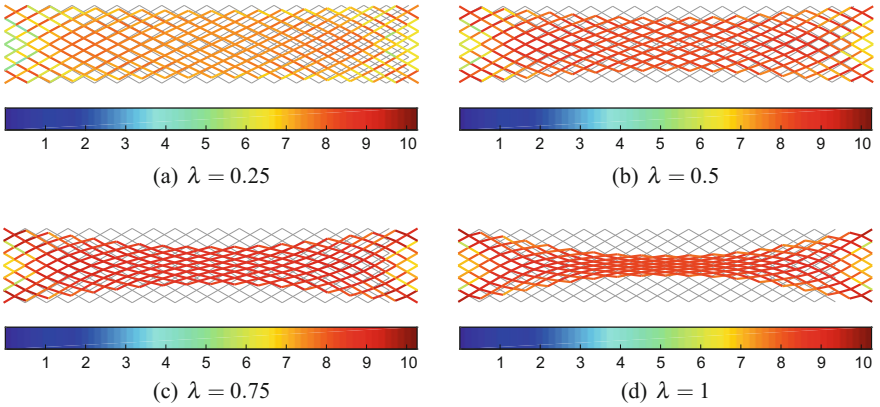

Fig. 13 Pantograph with non-orthogonal fibers ($\alpha_1 = \pi/6$): deformations by using the Hencky-type numerical model

Also in this case on the specimen was applied an assigned displacement on the right smaller side in the direction parallel to the larger sides until the value $u_{\max} = 74.7\,\text{mm}$ was reached. Three pictures were taken in the loading process (the strength machine and the velocity of the test are unchanged), see Fig. 16, corresponding to $\lambda = 0$, 0.5 and 1.

Numerical simulation of this experiment was performed using as springs stiffnesses those reported in Table 3. The results of the simulation are reported in Fig. 17, energies, structural reaction and density of structural reaction, and in Fig. 18, deformation history. We have to remark that in this case although there is a lack of closeness between the structural reaction given from the experiment and that computed numerically, mostly for values of $\lambda > 0.7$ (see Fig. 17b), the agreement on the whole set of displacement is again remarkable as can be observed by the overlapping of the two configurations at the final stage, see Fig. 19.

In our opinion this difference, unexpected if we consider the test with $\alpha_1 = \pi/6$, between the structural reaction evaluated in the experiment and computed numerically can be explained if we consider that in the $\alpha_1 = \pi/6$ test the ratio between the maximum assigned displacement and the long side, macro-strain, of the specimen is about 10% whereas the same quantity for the $\alpha_1 = \pi/3$ test is 53%. Looking again at Fig. 17b, if we consider only the first part of the curves (those corresponding approximatively to $\lambda \leq 0.4$) then there is a remarkable agreement between them. We highlight that $\lambda = 0.4$ corresponds to a macro-strain of about 21% less than half of that imposed on the specimen (53%).

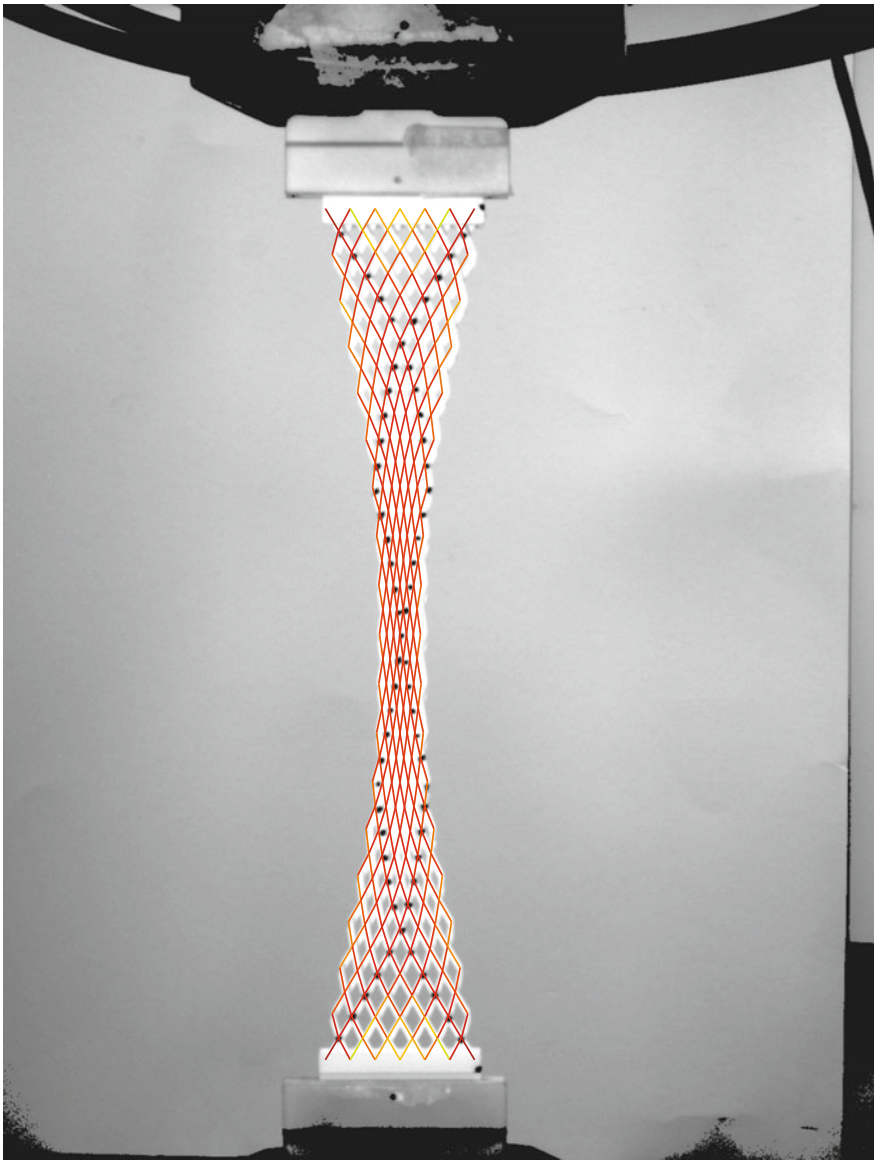

Fig. 14 Pantograph with non-orthogonal fibers ($\alpha_1 = \pi/6$): deformations by using the Hencky-type numerical model

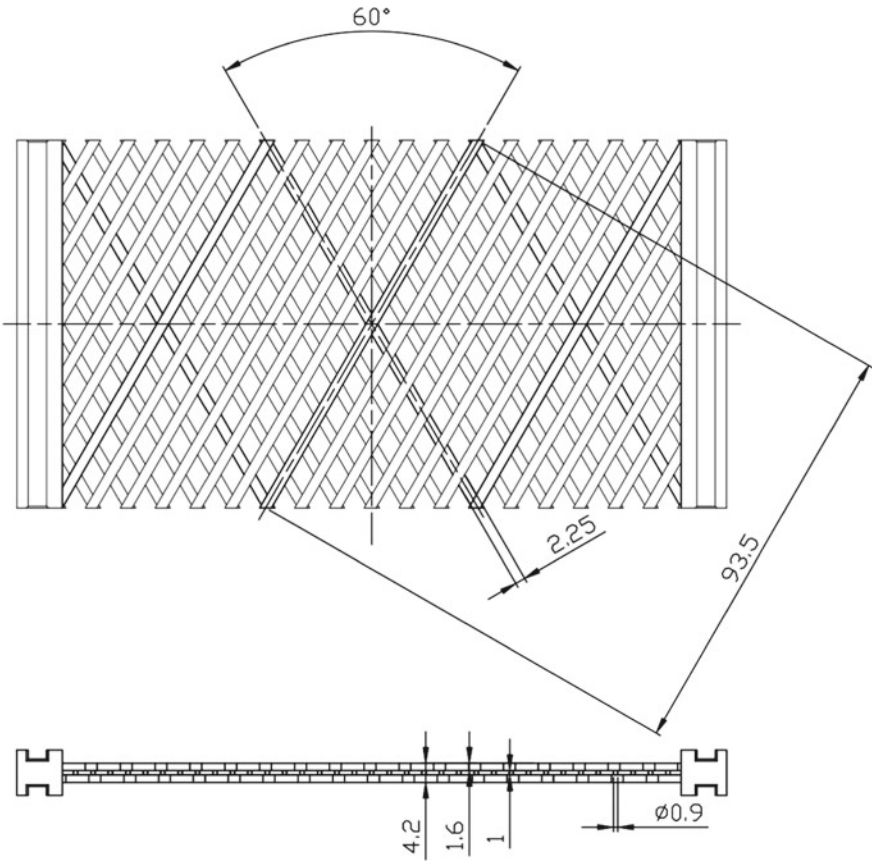

Fig. 15 Drawing of a pantographic structure with non-orthogonal fibers ($\alpha_1 = \pi/3$)

4 Concluding Remarks

In [5, 10, 14] more or less rigorous homogenization results are presented, in the framework of linear elasticity: i.e. small deformations and quadratic deformation energies. The model presented here, instead, tries to model the behavior of real pantographic structures undergoing large displacements. In the proposed experiments, while the majority of the beams constituting the pantographic lattice are in the small deformation regime, we can however distinguish some boundary layers in which the involved beam elements undergo very large deformations (more that 5% of elongations, for instance, as remarked in [3]). These experimental evidence compelled us to introduce strongly nonlinear models in order to be able to design a priori pantographic sheet having tailored properties.

While the numerical simulations show a surprising agreement with experimental evidence, we feel that a rigorous basis on the homogenization results presented in

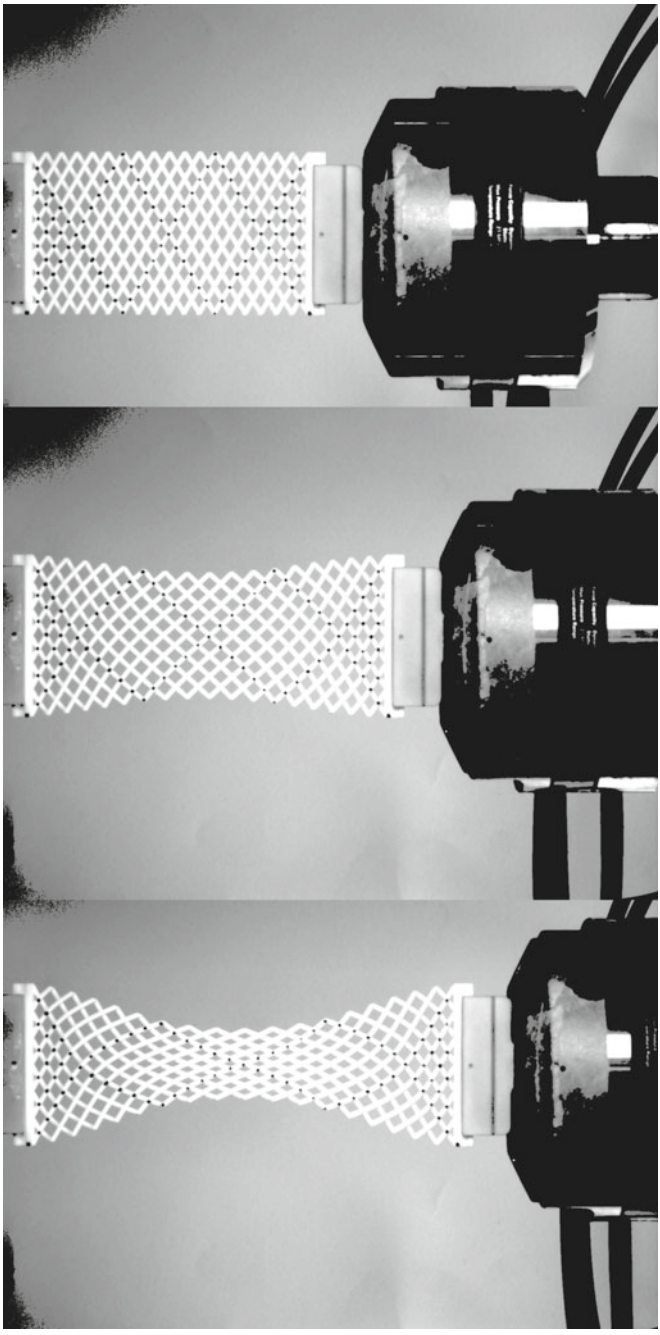

Fig. 16 Pantograph with non-orthogonal fibers ($\alpha_1 = \pi/3$): sequence of deformations for $\lambda = 0$, 0.5 and 1

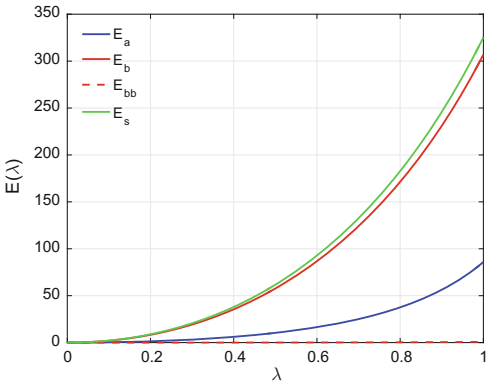

(a) Energy E *vs.* λ

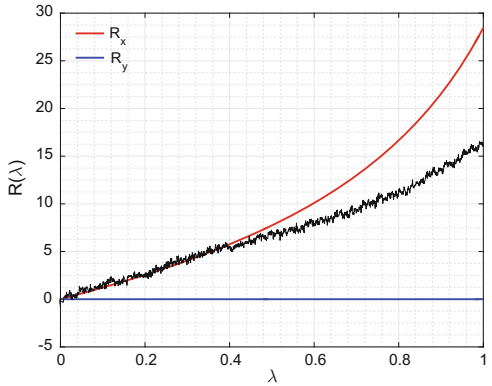

(b) Structural reaction R *vs.* λ
(in black is reported the experimental result)

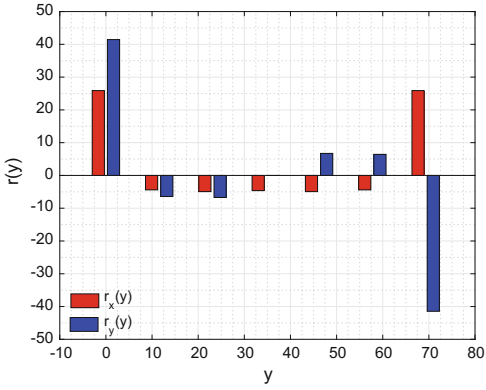

(c) Density of structural reaction r
on the side $x_1 = 0$ for $\lambda = 1$

Fig. 17 Pantograph with non-orthogonal fibers ($\alpha_1 = \pi/3$): energy, structural reaction and its density computed by using the Hencky-type numerical model

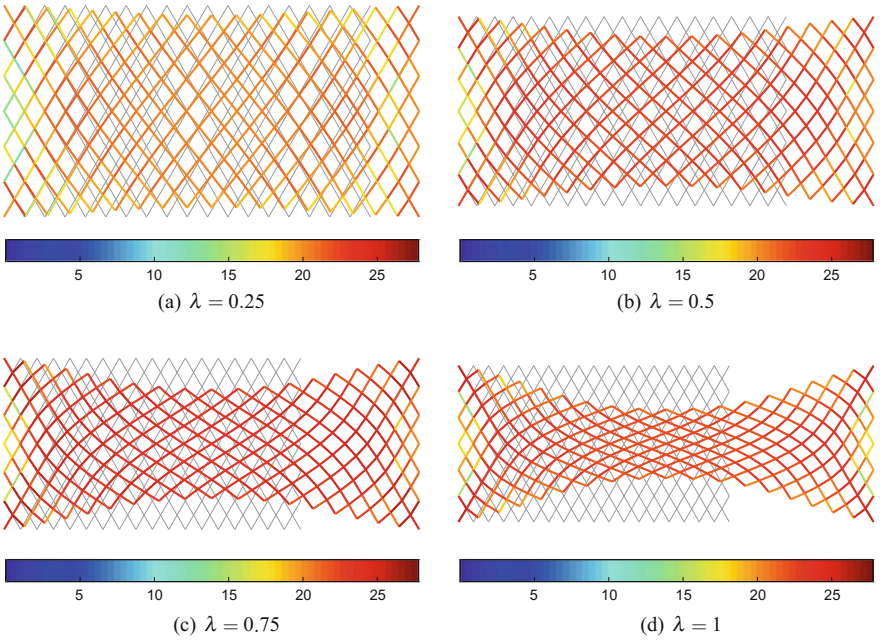

Fig. 18 Pantograph with non-orthogonal fibers ($\alpha_1 = \pi/3$): deformations by using the Hencky-type numerical model

[3] needs to be firmly established. We expect that Γ-convergence results can be now confidently formulated and conjectured, see [15]. Moreover we expect that the methods exploited in [16] could be adapted to get also a priori error estimates in the replacement process involved when passing from discrete to continuum models.

A final remark is needed: many cases of out of plane buckling of *exotic* pantographic sheets were observed. A phenomenological model proposed in [17, 18] has been successfully used to get qualitative predictions. However to get more general quantitative predictions an identification procedure involving discrete Lagrangian models with concentrated springs is needed, which applies to three-dimensional motion of two-dimensional pantographic sheets.

Future challenges concern:

i. Although pantographic structures were conceived to give an example of second gradient metamaterial, see e.g. [19–29], the development of 3D printing technology allowed for the *practical* synthesis of such metamaterials. It deserves to be investigated how to improve the design of 3D printed fabrics in order to fully exploit the exotic behaviour of higher gradient metamaterials. We remark that, as seen in [3, 30], the behaviour of higher gradient continua shows many peculiarities which deserve a deeper experimental investigation.
ii. The discrete nature of suitably designed beam lattices may be modelled also by means of more refined tools, see e.g. [31–38] for an in-depth description of

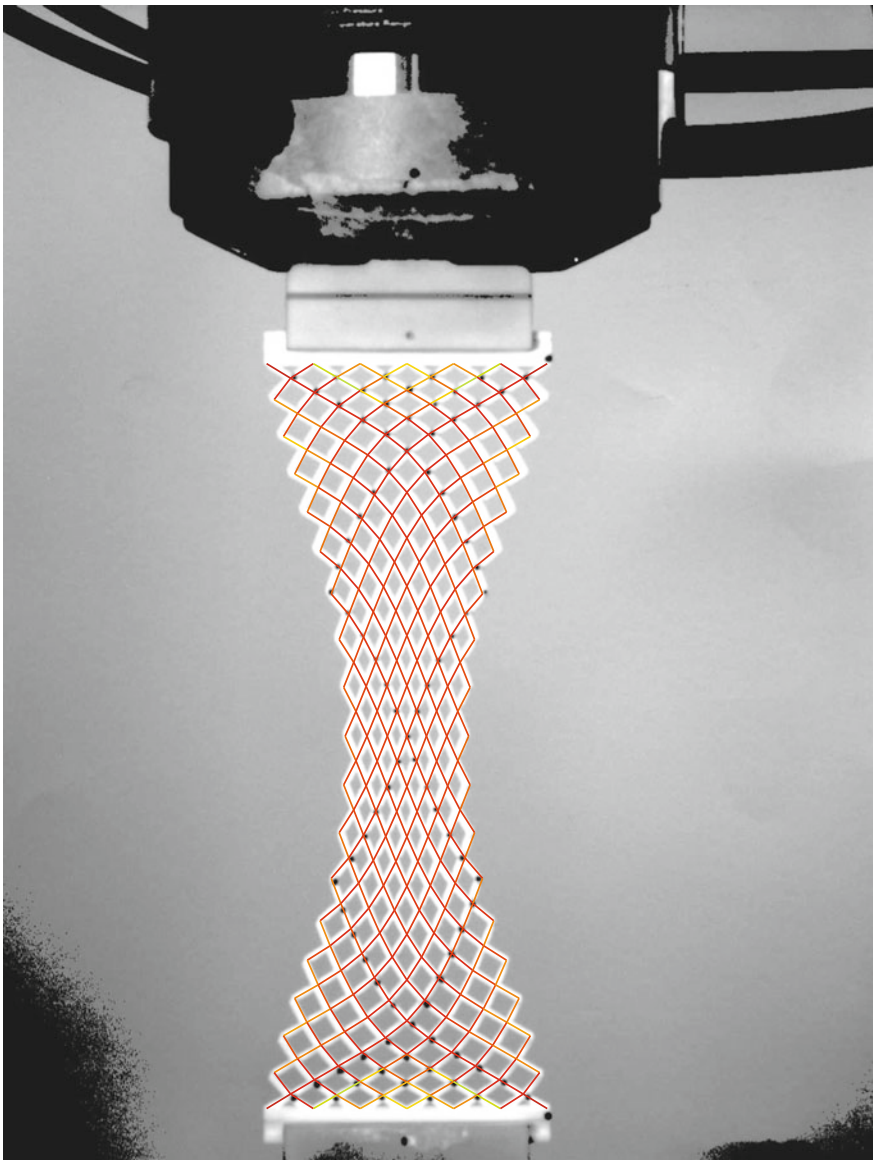

Fig. 19 Pantograph with non-orthogonal fibers ($\alpha_1 = \pi/3$): deformations by using the Hencky-type numerical model

NURBS interpolation or using the generalized beam theory, see [39, 40], this in order to design even more complex metamaterials also in the 3D case where could be efficiently used the Pipkin model described in [41] and in the review paper [42].

iii. Another crucial point concerns the modelling of the breakdown evolution of pantographic sheets. Indeed some evidence has been already gathered about the onset and the evolution of failure. It is rather evident that have to be considered ruptures concerning both fibers and pivots. A first modelling effort to model such rupture phenomena was presented in [43] when the attention was limited to the rupture mechanism initiated by the rupture of a fiber, see also [13] for an insight on the modelling of fiber defects. In this context, surely deserve models able to consider the out-of-plane deformations and the related buckling phenomena, see [44–48] for a quick insight on this argument.

iv. The experimental identification of the parameters of the discrete model, i.e. the stiffnesses of the springs, require a specific investigation (see [12]). In particular methods of best fitting must be coupled to those used in extended sensitivity analysis by adapting, for example, the tools described in [49] and exploited in [50–56], see also [57, 58] for a more specific application to the description of huge and innovative structures.

v. Experimental evidence shows the onset of some vibration phenomena in some specific experimental conditions. Therefore, it is relevant the extension of modelling to dynamic regimes, which can be obtained following the methods presented in see [59, 60] and also in [61, 62].

vi. The discrete Hencky-type model and the related numerical discretization technique could also be used to model granular media interactions, see [63], or generalized and micro-structured continua, see [19, 64–67] and, in particular, [68, 69] for applications in civil engineering and [70] in biomechanics.

vii. In various experiments the contact between fibers was observed; if this kind of phenomenon has to be considered they could be interesting the guidelines reported in [71, 72].

References

1. Turco, E., dell'Isola, F., Cazzani, A., Rizzi, N.L.: Hencky-type discrete model for pantographic structures: numerical comparison with second gradient continuum models. Zeitschrift für Angewandte Mathematik und Physik **67**(4), 1–28 (2016)
2. Hencky, H.: Über die angenäherte Lösung von Stabilitätsproblemen im Raum mittels der elastischen Gelenkkette. Ph.D. thesis, Engelmann (1921)
3. dell'Isola, F., Giorgio, I., Pawlikowski, M., Rizzi, N.L.: Large deformations of planar extensible beams and pantographic lattices: heuristic homogenisation, experimental and numerical examples of equilibrium. Proc. R. Soc. Lond. A: Math. Phys. Eng. Sci. **472**(2185) (2016)
4. dell'Isola, F., Lekszycki, T., Pawlikowski, M., Grygoruk, R., Greco, L.: Designing a light fabric metamaterial being highly macroscopically tough under directional extension: first experimental evidence. Zeitschrift für angewandte Mathematik und Physik **66**(6), 3473–3498 (2015)
5. Alibert, J.-J., Seppecher, P., dell'Isola, F.: Truss modular beams with deformation energy depending on higher displacement gradients. Math. Mech. Solids **8**(1), 51–73 (2003)
6. Madeo, A., Della Corte, A., Greco, L., Neff, P.: Wave propagation in pantographic 2D lattices with internal discontinuities. Proc. Est. Acad. Sci. **64**(3S), 325–330 (2015)

7. Turco, E., Golaszewski, M., Cazzani, A., Rizzi, N.L.: Large deformations induced in planar pantographic sheets by loads applied on fibers: experimental validation of a discrete Lagrangian model. Mech. Res. Commun. **76**, 51–56 (2016)
8. Turco, E., Barcz, K., Pawlikowski, M., Rizzi, N.L.: Non-standard coupled extensional and bending bias tests for planar pantographic lattices. Part I: numerical simulations. Zeitschrift für Angewandte Mathematik und Physik **67**(122), 1–16 (2016)
9. Turco, E., Barcz, K., Rizzi, N.L.: Non-standard coupled extensional and bending bias tests for planar pantographic lattices. Part II: comparison with experimental evidence. Zeitschrift für Angewandte Mathematik und Physik **67**(123), 1–16 (2016)
10. Alibert, J.-J., Della Corte, A.: Second-gradient continua as homogenized limit of pantographic microstructured plates: a rigorous proof. Zeitschrift für Angewandte Mathematik und Physik **66**(5), 2855–2870 (2015)
11. Pideri, C., Seppecher, P.: A second gradient material resulting from the homogenization of an heterogeneous linear elastic medium. Contin. Mech. Thermodyn. **9**(5), 241–257 (1997)
12. Placidi, L., Andreaus, U., Della Corte, A., Lekszycki, T.: Gedanken experiments for the determination of two-dimensional linear second gradient elasticity coefficients. Zeitschrift für Angewandte Mathematik und Physik (ZAMP) **66**(6), 3699–3725 (2015)
13. Turco, E., Rizzi, N.L.: Pantographic structures presenting statistically distributed defects: numerical investigations of the effects on deformation fields. Mech. Res. Commun. **77**, 65–69 (2016)
14. Boutin, C., dell'Isola, F., Giorgio, I., Placidi, L.: Linear pantographic sheets. Part I: asymptotic micro-macro models identification. Mathematics and Mechanics of Complex Systems (in press)
15. Braides, A., Solci, M.: Asymptotic analysis of Lennard-Jones systems beyond the nearest-neighbour setting: a one-dimensional prototypical case. Math. Mech. Solids **21**(8), 915–930 (2016)
16. Carcaterra, A., dell'Isola, F., Esposito, R., Pulvirenti, M.: Macroscopic description of microscopically strongly inhomogenous systems: a mathematical basis for the synthesis of higher gradients metamaterials. Arch. Rational Mech. Anal. (2015). doi:10.1007/s00205-015-0879-5
17. Steigmann, D.J., dell'Isola, F.: Mechanical response of fabric sheets to three-dimensional bending, twisting, and stretching. Acta Mech. Sin. **31**(3), 373–382 (2015)
18. Scerrato, D., Giorgio, I., Rizzi, N.L.: Three-dimensional instabilities of pantographic sheets with parabolic lattices: numerical investigations. Zeitschrift für Angewandte Mathematik und Physik **67**(3), 1–19 (2016)
19. dell'Isola, F., Steigmann, D., Della Corte, A.: Synthesis of fibrous complex structures: designing microstructure to deliver targeted macroscale response. Appl. Mech. Rev. **67**(6), 060804 (2015)
20. Giorgio, I., Grygoruk, R., dell'Isola, F., Steigmann, D.J.: Pattern formation in the three-dimensional deformations of fibered sheets. Mech. Res. Commun. **69**, 164–171 (2015)
21. Scerrato, D., Giorgio, I., Della Corte, A., Madeo, A., Limam, A.: A micro-structural model for dissipation phenomena in the concrete. Int. J. Numer. Anal. Methods Geomech. **39**(18), 2037–2052 (2015)
22. Scerrato, D., Zhurba Eremeeva, I.A., Lekszycki, T., Rizzi, N.L.: On the effect of shear stiffness on the plane deformation of linear second gradient pantographic sheets. Zeitschrift für Angewandte Mathematik und Mechanik (2016). doi:10.1002/zamm.201600066
23. D'Agostino, M.V., Giorgio, I., Greco, L., Madeo, A., Boisse, P.: Continuum and discrete models for structures including (quasi-) inextensible elasticae with a view to the design and modeling of composite reinforcements. Int. J. Solids Struct. **59**, 1–17 (2015)
24. Placidi, L., Andreaus, U., Giorgio, I.: Identification of two-dimensional pantographic structure via a linear d4 orthotropic second gradient elastic model. J. Eng. Math. (2017). doi:10.1007/s10665-016-9856-8
25. Placidi, L., Dhaba, A.E.: Semi-inverse method à la Saint-Venant for two-dimensional linear isotropic homogeneous second-gradient elasticity. Math. Mech. Solids (2017). doi:10.1177/1081286515616043

26. dell'Isola, F., Giorgio, I., Andreaus, U.: Elastic pantographic 2d lattices: a numerical analysis on static response and wave propagation. Proc. Est. Acad. Sci. **64**(3), 219–225 (2015)
27. dell'Isola, F., Della Corte, A., Greco, L., Luongo, A.: Plane bias extension test for a continuum with two inextensible families of fibers: a variational treatment with Lagrange multipliers and a perturbation solution. Int. J. Solids Struct. **81**, 1–12 (2016)
28. Cuomo, M., dell'Isola, F., Greco, L.: Simplified analysis of a generalized bias test for fabrics with two families of inextensible fibres. Zeitschrift für angewandte Mathematik und Physik **67**(3), 1–23 (2016)
29. dell'Isola, F., Cuomo, M., Greco, L., Della Corte, A.: Bias extension test for pantographic sheets: numerical simulations based on second gradient shear energies. J. Eng. Math. (2017). doi:10.1007/s10665-016-9865-7
30. dell'Isola, F., Andreaus, U., Placidi, L.: At the origins and in the vanguard of peridynamics, non-local and higher-gradient continuum mechanics: an underestimated and still topical contribution of Gabrio Piola. Math. Mech. Solids **20**(8), 887–928 (2015)
31. Cazzani, A., Malagù, M., Turco, E.: Isogeometric analysis of plane curved beams. Math. Mech. Solids **21**(5), 562–577 (2016)
32. Cazzani, A., Malagù, M., Turco, E.: Isogeometric analysis: a powerful numerical tool for the elastic analysis of historical masonry arches. Contin. Mech. Thermodyn. **28**(1), 139–156 (2016)
33. Cazzani, A., Malagù, M., Turco, E., Stochino, F.: Constitutive models for strongly curved beams in the frame of isogeometric analysis. Math. Mech. Solids **21**(2), 182–209 (2016)
34. Bilotta, A., Formica, G., Turco, E.: Performance of a high-continuity finite element in three-dimensional elasticity. Int. J. Numer. Methods Biomed. Eng. **26**, 1155–1175 (2010)
35. Greco, L., Cuomo, M.: B-spline interpolation of Kirchhoff-Love space rods. Comput. Methods Appl. Mech. Eng. **256**, 251–269 (2013)
36. Greco, L., Cuomo, M.: An implicit G^1 multi patch B-spline interpolation for Kirchhoff-Love space rod. Comput. Methods Appl. Mech. Eng. **269**, 173–197 (2014)
37. Greco, L., Cuomo, M.: An isogeometric implicit G1 mixed finite element for Kirchhoff space rods. Comput. Methods Appl. Mech. Eng. **298**, 325–349 (2016)
38. Cazzani, A., Stochino, F., Turco, E.: An analytical assessment of finite elements and isogeometric analysis of the whole spectrum of Timoshenko beams. Zeitschrift für Angewandte Mathematik und Mechanik **96**(10), 1220–1244 (2016)
39. Piccardo, G., Ranzi, G., Luongo, A.: A complete dynamic approach to the generalized beam theory cross-section analysis including extension and shear modes. Math. Mech. Solids **19**(8), 900–924 (2014)
40. Piccardo, G., Ranzi, G., Luongo, A.: A direct approach for the evaluation of the conventional modes within the gbt formulation. Thin-Walled Struct. **74**, 133–145 (2014)
41. Placidi, L., Greco, L., Bucci, S., Turco, E., Rizzi, N.L.: A second gradient formulation for a 2D fabric sheet with inextensible fibres. Zeitschrift für angewandte Mathematik und Physik **67**(114), 1–24 (2016)
42. Placidi, L., Barchiesi, E., Turco, E., Rizzi, N.L.: A review on 2D models for the description of pantographic fabrics. Zeitschrift für angewandte Mathematik und Physik **67**(121), 1–20 (2016)
43. Turco, E., dell'Isola, F., Rizzi, N.L., Grygoruk, R., Müller, W.H., Liebold, C.: Fiber rupture in sheared planar pantographic sheets: numerical and experimental evidence. Mech. Res. Commun. **76**, 86–90 (2016)
44. D'Annibale, F., Rosi, G., Luongo, A.: Linear stability of piezoelectric-controlled discrete mechanical systems under nonconservative positional forces. Meccanica **50**(3), 825–839 (2015)
45. Rizzi, N., Varano, V., Gabriele, S.: Initial postbuckling behavior of thin-walled frames under mode interaction. Thin-Walled Struct. **68**, 124–134 (2013)
46. Gabriele, S., Rizzi, N., Varano, V.: A 1D higher gradient model derived from Koiter's shell theory. Math. Mech. Solids **21**(6), 737–746 (2016)
47. AminPour, H., Rizzi, N.: A one-dimensional continuum with microstructure for single-wall carbon nanotubes bifurcation analysis. Math. Mech. Solids **21**(2), 168–181 (2016)

48. Gabriele, S., Rizzi, N.L., Varano, V.: A 1D nonlinear TWB model accounting for in plane cross-section deformation. Int. J. Solids Struct. **94–95**, 170–178 (2016)
49. Turco, E.: Tools for the numerical solution of inverse problems in structural mechanics: review and research perspectives. Eur. J. Environ. Civil Eng. 1–46 (2017). doi:10.1080/19648189.2015.1134673
50. Lekszycki, T., Olhoff, N., Pedersen, J.J.: Modelling and identification of viscoelastic properties of vibrating sandwich beams. Compos. Struct. **22**(1), 15–31 (1992)
51. Bilotta, A., Turco, E.: A numerical study on the solution of the Cauchy problem in elasticity. Int. J. Solids Struct. **46**, 4451–4477 (2009)
52. Bilotta, A., Morassi, A., Turco, E.: Reconstructing blockages in a symmetric duct via quasi-isospectral horn operators. J. Sound Vib. **366**, 149–172 (2016)
53. Bilotta, A., Turco, E.: Numerical sensitivity analysis of corrosion detection. Math. Mech. Solids. **22**(1), 72–88 (2017). doi:10.1177/1081286514560093
54. Alessandrini, G., Bilotta, A., Formica, G., Morassi, A., Rosset, E., Turco, E.: Evaluating the volume of a hidden inclusion in an elastic body. J. Comput. Appl. Math. **198**(2), 288–306 (2007)
55. Alessandrini, G., Bilotta, A., Morassi, A., Turco, E.: Computing volume bounds of inclusions by EIT measurements. J. Sci. Comput. **33**(3), 293–312 (2007)
56. Turco, E.: Identification of axial forces on statically indeterminate pin-jointed trusses by a nondestructive mechanical test. Open Civ. Eng. J. **7**, 50–57 (2013)
57. Buffa, F., Cazzani, A., Causin, A., Poppi, S., Sanna, G.M., Solci, M., Stochino, F., Turco, E.: The Sardinia radio telescope: a comparison between close range photogrammetry and FE models. Math. Mech. Solids 1–22 (2015). doi:10.1177/1081286515616227
58. Stochino, F., Cazzani, A., Poppi, S., Turco, E.: Sardinia radio telescope finite element model updating by means of photogrammetric measurements. Math. Mech. Solids 1–17 (2015). doi:10.1177/1081286515616046
59. Del Vescovo, D., Giorgio, I.: Dynamic problems for metamaterials: review of existing models and ideas for further research. Int. J. Eng. Sci. **80**, 153–172 (2014)
60. Battista, A., Cardillo, C., Del Vescovo, D., Rizzi, N.L., Turco, E.: Frequency shifts induced by large deformations in planar pantographic continua. Nanomech. Sci. Technol.: Int J. **6**(2), 161–178 (2015)
61. Cazzani, A., Stochino, F., Turco, E.: On the whole spectrum of Timoshenko beams. Part I: a theoretical revisitation. Zeitschrift für Angewandte Mathematik und Physik **67**(24), 1–30 (2016)
62. Cazzani, A., Stochino, F., Turco, E.: On the whole spectrum of Timoshenko beams. Part II: further applications. Zeitschrift für Angewandte Mathematik und Physik **67**(25), 1–21 (2016)
63. Misra, A., Poorsolhjouy, P.: Granular micromechanics based micromorphic model predicts frequency band gaps. Contin. Mech. Thermodyn. **28**(1), 215–234 (2016)
64. Altenbach, J., Altenbach, H., Eremeyev, V.A.: On generalized Cosserat-type theories of plates and shells: a short review and bibliography. Arch. Appl. Mech. **80**(1), 73–92 (2010)
65. Eremeyev, V.A., Pietraszkiewicz, W.: Material symmetry group and constitutive equations of micropolar anisotropic elastic solids. Math. Mech. Solids. **21**(2), 210–221 (2016). doi:10.1177/1081286515582862
66. Dos Reis, F., Ganghoffer, J.F.: Construction of micropolar continua from the asymptotic homogenization of beam lattices. Comput. Struct. **112–113**, 354–363 (2012)
67. Elnady, K., Dos Reis, F., Ganghoffer, J.-F.: Construction of second order gradient continuous media by the discrete asymptotic homogenization method. Int. J. Appl. Mech. (2014)
68. Caggegi, C., Pensée, V., Fagone, M., Cuomo, M., Chevalier, L.: Experimental global analysis of the efficiency of carbon fiber anchors applied over CFRP strengthened bricks. Constr. Build. Mater. **53**, 203–212 (2014)
69. Tedesco, F., Bilotta, A., Turco, E.: Multiscale 3D mixed FEM analysis of historical masonry constructions. Eur. J. Environ. Civ. Eng. (2017). doi:10.1080/19648189.2015.1134676
70. Tomic, A., Grillo, A., Federico, S.: Poroelastic materials reinforced by statistically oriented fibres - numerical implementation and application to articular cartilage. IMA J. Appl. Math. **79**, 1027–1059 (2014)

71. Andreaus, U., Chiaia, B., Placidi, L.: Soft-impact dynamics of deformable bodies. Contin. Mech. Thermodyn. **25**, 375–398 (2013)
72. Andreaus, U., Baragatti, P., Placidi, L.: Experimental and numerical investigations of the responses of a cantilever beam possibly contacting a deformable and dissipative obstacle under harmonic excitation. Int. J. Non-Linear Mech. **80**, 96–106 (2016)